Thai Geoscience Journal 4(5), 2023, p. 1 - 10

ISSN-2730-2695; DOI-10.14456/tgj.2023.1

Subsidence Susceptibility Mapping in Tropical Island Karst: A comparison of approaches used in the Municipality of General Luna in Siargao Island, Philippines

Hugo, Marie Krystel D.[1,2], Agot, Ross Dominic D. [1,2], Manzano, Liza Socorro J. [1*], Esmeralda, Aquila Kristian B.[1], Abracia, Aaron Miguel C.[1], Madrigal, Madonna Feliz B. [1,2], Ondona, April C. [1], Dela Torre, Angelo Ma. Gabriel P.[1], Isip, Marcius Elaeo G.[1], Rivera, John Michael D.[1], Umali, Julius Vincent P. [1], Belesario, Nelgie Ann C.[1]

[1] *Department of Environment and Natural Resources – Mines and Geosciences Bureau (DENR – MGB), Quezon City, Philippines*
[2] *University of the Philippines - Diliman, Quezon City, Philippines*
*****Corresponding author: lizajmanzano@yahoo.com*
Received 26 December 2022; Accepted 8 June 2023.

Abstract

Karst subsidence hazard susceptibility mapping is an integral part of the National Geohazards Assessment and Mapping Program (NGAMP) initiated by the Mines and Geosciences Bureau (MGB) in 2013. It aims to comprehensively assess geohazards in karst regions in the Philippines. The mapping process involves three primary procedures: remote sensing interpretation of IfSAR-derived Sink Depth Maps using ArcGIS, geological and geomorphological assessment, and geophysical survey using Ground Penetrating Radar (GPR). This method considers sinkhole distribution, other karst features, ground movement evidence, and GPR survey results to identify subsidence-prone areas. The approach generates Karst Subsidence Susceptibility Maps indicating highly vulnerable regions, considering the unpredictable nature of sinkhole collapse.

To enhance the methodology and susceptibility classifications, the PhilKARST Program of MGB introduced the statistical Weights of Evidence (WoE) analysis and employed in General Luna, a prominent tourist destination in Siargao Island, Philippines. This approach ensures consistency and reproducibility by examining the correlation between hazard inventories and fifteen (15) conditional factors.

The resultant weights are determined to generate a subsidence susceptibility index map with Low, Moderate, High, and Very High ratings. Evaluation of true- and false-positive rates using available training data indicated an initial success rate of 82.2% for subsidence susceptibility modeling, signifying reliable results. The enhanced susceptibility map for General Luna in Surigao del Norte, displays lower susceptibility classifications in areas with fewer or no sinkhole occurrences. This differs from the output map of the previous method, which exclusively highlighted highly susceptible areas based on sinkhole distribution, other karstic features, and GPR surveys.

Keywords: Geohazards, Karst, Subsidence, Susceptibility Mapping, Sustainable Tourism

1. Introduction

Karst topography covers a significant land area in the Philippines. Previous studies such as that of Piccini and Rossi (1994) mention that about 10% of around 30,000 km^2 of the Philippine land surface is characterized by karst topography composed of outcrops that are generally smaller than 100 km^2. Most related published papers characterize and describe karst in the Philippines from speleological expeditions in Luzon, Samar, and Palawan in the 1970s and 1980s (Piccini and Rossi, 1994). In October 2013, the M_w7.2 Bohol earthquake struck and exposed numerous sinkholes in southwestern Bohol causing damages to communities, infrastructures, and the natural environment (Mines and Geosciences Bureau [MGB], 2015)

Responding to the need for a comprehensive geohazard assessment of areas characterized by karst topography as unraveled by the Bohol Earthquake, the MGB expands its National Geohazard Mapping and Assessment Program (NGAMP) to include Karst Subsidence hazards due to sinkhole collapse. It aims to identify areas that are susceptible to the said hazard, to make this information available to Local Government Units (LGUs) through the generation of karst subsidence hazard maps and technical reports, and to promote public awareness for proper prevention and mitigation measures against karst subsidence due to sinkhole collapse. As of 2022, the project targets 1,183 cities and municipalities identified to be underlain by carbonate rocks, formations with calcareous sedimentary members, and recent deposits based on compiled data in the Geology of the Philippines (MGB, 2010). One of the accomplished sites is the Municipality of General Luna, Surigao del Norte, which was assessed in 2019 following the established methodology discussed in the project guidebook. This includes gathering of anecdotal accounts, interpretation of satellite data from the Interferometric Synthetic Aperture Radar (IfSAR) and Light Detection and Ranging (LiDAR) Digital Elevation Models, geologic and geomorphic studies, establishment of a sinkhole inventory, Ground Penetrating Radar (GPR) surveys, and the conduct of an IEC Campaign to local authorities.

Despite this, there is still a lack of understanding on their occurrence and the factors that contribute to sinkhole evolution that may lead to a largely overestimated hazard susceptibility zonation, which may hamper development or result in erroneous disaster risk reduction planning. Hence, to enhance its karst subsidence hazard assessment campaign, the Climate--responsive Karst Management for Sustainable Tourism (PhilKARST Program) is implemented from 2021 until 2023. This involves not only the updating of available subsidence hazard inventories, structural and geomorphological mapping but also statistical analyses and model validation. The outputs and methodologies formulated for hazard assessment seek to pave the way for objective decision-making, especially for sustainable tourism. This program has three (3) pilot study areas that are considered as developed and developing karst tourism sites in the country but highlighted in this paper is the Municipality of General Luna in Siargao Island, Surigao del Norte. This municipality is situated at the southeastern tip of the island facing the Pacific Ocean at its east.

Geology and Geomorphology of General Luna, Siargao Island

According to Fernandez, H. (1966), Siargao Island is underlain by the Cretaceous to Paleogene (?) Sapao Formation – the primary igneous rock sequence composed of spilitic basalt and diabase at the northern portion of the island – and the Miocene to Pleistocene Siargao Formation that comprises limestone and clastics underlying most of General Luna. The younger Pleistocene member was said to overlie the Miocene units without hiatus (MGB, 2019). The samples analyzed by PhilKARST, through petrographic and paleontological techniques, generally contain small and large benthic foraminifera, red algae, echinoid spine, coral fragments, gastropod, ostracod, and mollusk fragments deposited along the foreslope and shallow neritic environments. The occurrence of *Miogypsina sp.* suggests an Early to Middle Miocene age. Lastly, some portions of the municipality are capped by thick non-calcareous clastics.

Siargao Island is seismically active as it lies between two major structures namely the Mindanao segment of the Philippine Fault to its west and the Philippine Trench to its east (MMAJ-JICA, 1990). Moreover, major northwest-trending faults influenced the lithologic distribution along these islands and are complemented by northeast-trending lineaments. These are also observed in all lithologic units within the municipality. Movement observed along identified faults within the study area is evidenced by slickensides and displacement along reef flats (MGB, 2019).

General Luna is defined by old platform limestone ridges and cockpit topography at its west, undulating clastic hills, younger hillocks, valley flats towards its central portion, wide beaches, and reef flats along with distributed mangrove forests along its coastal zones to the east (MGB, 2019). This constitutes different levels or episodes of karstification that are also

defined by the active seismicity in the area. Cave networks and sinkhole formation are also evident throughout the karst landscapes in the municipality.

2. Materials and Methods

NGAMP: Karst Subsidence Hazards Assessment and Mapping

Three (3) primary procedures were employed to generate a Karst Subsidence Susceptibility Map: (a) remote sensing interpretation of IfSAR-derived Sink Depth Map (Fig. 1) processed using ArcGIS tools, (b) geological and geomorphological assessment, and (c) geophysical survey using the Ground Penetrating Radar (GPR).

a. Remote Sensing Interpretation

Prior to the field assessment, MGB uses the IfSAR derived Digital Elevation Model (DEM) to determine the location of possible sinkholes and terrain attributes (MGB, 2015). Using the ArcGIS hydrologic toolset, raw elevation data was pre-processed or reconditioned to extract karst depression features through a step-by-step procedure. It starts with the generation of flow directions in the area. Then, the Watershed tool is utilized to determine sink areas or "catchments" from the steepest downslope neighbor of each cell. To achieve the raster of minimum and maximum elevations of the watershed for each sink, Zonal Statistics, and Zonal Fill tools are applied. Ultimately, using Minus, the minimum values will be subtracted to maximum values and generate a "fill-difference" raster that represents the varying depth of depressions in the original surface. The generated sinks are superimposed on the topographic map and classified into corresponding depth ranges suitable to the terrain of the study area (Garas et.al, 2020). These generated "sinks" were the basis during the field survey in all barangays.

b. Geological and Geomorphological Assessment

A field survey was conducted in all accessible villages (hereinafter referred to as barangays) and islands within the Municipality of General Luna. The extent and distribution of the different lithological units based on existing 1:50,000-scale Geologic Maps of Siargao were validated. The different karst and non-karst landforms were also delineated based on ground observations and DEM interpretation.

Following this, an inventory of karst features (i.e., sinkholes, cave openings, springs) was also established by ground validation. A matrix of karst features, including assessed and IfSAR-derived sinkholes and other observed features, was prepared with the following information: a) location, b) type of sinkhole, c) morphometry, d) observations on the geology and geomorphology of the vicinity.

c. Geophysical Survey using the Ground Penetrating Radar (GPR)

A Ground Penetrating Radar (GPR) survey was conducted in pre-selected sites based on the selection criteria established by MGB (MGB Karst Guidebook, 2015). Data is collected using the Geophysical Survey Systems, Inc. (GSSI) SIR 3000 paired with the Multiple Low Frequency (MLF) 80 MHz antenna reaching depths up to 25 meters. These are then processed using the RADAN 7 Software and finalized with Transfer Spectrum tool.

The generated radargrams show distinct subsurface layers, in differing sizes and depths, as indicated by the anomalies. These anomalies are represented by various colors assigned during radargram processing. Voids or cavities appear in red, saturated layers are green and yellow as solid material or carbonate rock units. The colors can also be representative of possible cave systems, subterranean drainage pathways, buried sinkholes, and geologic structures that transcend underneath the area of interest.

d. Generation of MGB's Karst Subsidence Susceptibility Map

The results of the remote sensing interpretation and the geological and geomorphological datasets were combined to generate the susceptibility map. This method applied an expert's opinion approach, such that the delineation of areas susceptible were based on the following:1) the distribution of karst features,

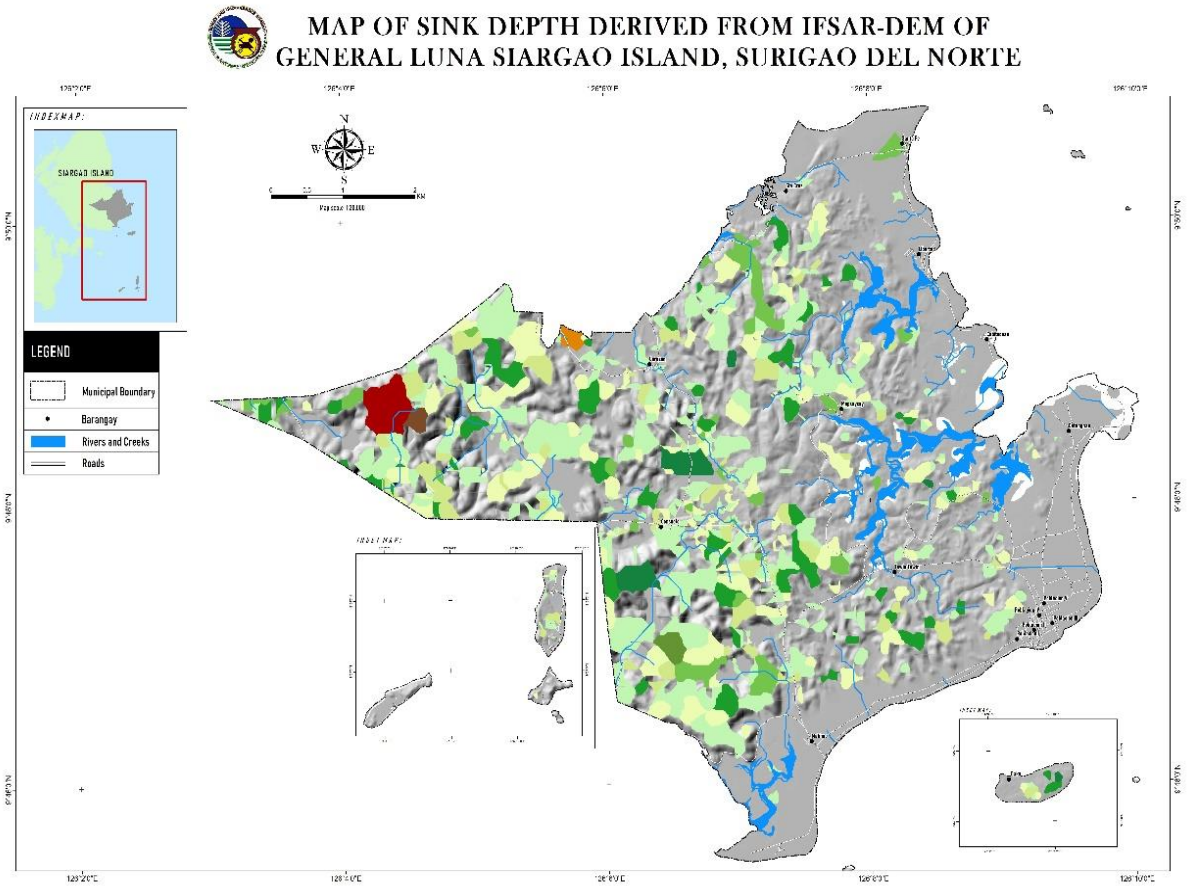

Fig. 1: Sink Depth Map of the study area generated from IfSAR-DEM.

2) subsurface configuration, 3) lithologic and geomorphic characteristics,4) surface mass movement (e.g., rock fall, slump), 5) shallow wells, and 6) other geologic structures (e.g., joints, faults, lineaments). Other parameters considered were the presence of differential settlements, heaving, progress-sing tension cracks, subsiding road surfaces, and staircase and horizontal cracks in concrete structures.

Enhancement of the Subsidence Susceptibility Mapping using an integrated statistical approach

a. Preparation of sinkhole inventory

The sinkhole inventory of General Luna, Surigao Del Norte was compiled from existing records obtained in previous field investigations. The sinkhole dataset was split into training and testing subsets with a 70-30 ratio, respectively. The training subset was used to create the susceptibility model, while the testing subset was used for validation. These subsets were then converted into raster format. The raster pixels were assigned the values of 1 for the presence and 0 for the absence of sinkholes.

b. Generation of sinkhole-conditioning factor maps

Several factors identified from related literature were tested for their influence on sinkhole formation (Table 1). Most factor layers were derived from existing datasets from the government and other organizations, although some were obtained from publicly available sources. The factor layers in shapefile format were converted to .tiff format to allow for analysis of pixel distribution. Each factor was divided into classes based on their attributes and reclassified, with an assigned integer value for the pixels of each class (Table 2).

Table 1. Factors identified from related literature with the corresponding sources and processing data.

Factor	Source	Remarks
Geomorphological Factors (Elevation, Slope, Aspect, Curvature)	Derived from IfSAR-DEM (NAMRIA, 2013)	5-meter resolution
Sinkhole Density and Proximity	Existing MGB Central and Regional Offices inventories; other agencies	Processed using ArcMap tools
Lineament Density and Proximity		
Cave Density		
Springs and Wells Density		
Proximity to Drainage	IfSAR-DEM generated using ArcMap tools	
Geology/Lithology	PhilKARST Program Project 1	
Geomorphology		
Land Cover	ESA WorldCover	10-meter resolution
NDVI	Sentinel-2	

Table 2. Assigned integer value for the pixels of each factor class

		Factor class	
		Present	Absent
Hazard	Present	Npix1	Npix2
	Absent	Npix3	Npix4

c. Determination of factor significance

The factor map and inventory raster data prepared were then imported into the Integrated Land and Water Information System (ILWIS) program for statistical analysis. The hazard inventory was overlapped with the factor maps to determine the distribution of the hazard pixels for each class. The weights for each class are then calculated using the formula for Weight of Evidence as shown below:

$$W^+ = ln\frac{\frac{Npix_1}{Npix_1 + Npix_2}}{\frac{Npix_3}{Npix_3 + Npix_4}} \qquad W^- = ln\frac{\frac{Npix_2}{Npix_1 + Npix_2}}{\frac{Npix_4}{Npix_3 + Npix_4}}$$

Where:

W^+ = effect of the factor's presence
W^- = effect of the factor's absence
N_{pix} = number of pixels where both hazards and factor occur

$$W_{map} = W^+ + W_{minSum} - W^-$$

The resultant weights were tabulated, and classes with positive values were considered favorable to hazard occurrence, while those with negative values were considered unfavorable. Favorable pixels that overlapped with hazard pixels were considered true positives, while those that overlapped non-hazard pixels were considered false positives. Likewise, unfavorable pixels that overlapped with non-hazard pixels were considered true negatives, while those that overlapped hazard pixels were considered false negatives. These values were used to compute True- and False-positive rates (TFR and TPR) using Microsoft Excel with the formulas below. These were then graphed to measure the Area-Under-the-Curve (AUC). Factors with AUC values above 0.6 were considered significant and included in the final calculation of susceptibility index values.

$$TPR = \frac{TP}{TP + FN}$$

$$FPR = \frac{FP}{FP + TN}$$

d. Generation of the enhanced karst subsidence susceptibility map

The weighted raster maps of the six (6) significant factors were superimposed on one another using ILWIS. Weight values were then added for each pixel to produce a raw susceptibility index map. These were subsequently normalized within 0 to 100 values. Using these, a test run was done to determine threshold values for susceptibility zonation

based on the frequency of intersecting hazard pixels.

The very high and high susceptibility classes were then assigned 50% and 30% of the hazard pixels, respectively. Moderate Susceptibility was set to 15% of the hazard pixels, while low contained 5% hazard pixels. True- and False--positive rates were calculated using the training and testing subsets to obtain the AUC for the success and prediction rates. The output map was further cleansed and smoothened to provide a more logical and visual image for stakeholders.

3. Results and Discussion

Sinkhole and Karst Features Inventory

A total of 381 sinkholes based on ground validation, IfSAR interpretation, and the topographic map delineation by the National Mapping and Resource Information Authority (NAMRIA) was plotted in the MGB Karst Subsidence Susceptibility Map. The ground validated sinkholes included in the inventory are 302 karst sinkholes of various types and 20 pseudokarst sinkholes considering that there are areas with tuffaceous clastics underlain by limestone. The aperture sizes range from 1 meter to 300 meters while depths range from 0.1 to 3 meters (MGB, 2019). There were 161 caves and cave openings identified in different barangays. On the other hand, a total of 248 ground-validated karst sinkhole polygons comprised the hazard layer used in the enhanced subsidence susceptibility model. Fewer sinkholes were included in the said model due to the presence of sinkholes plotted as points which have limitations in the resolution.

The previous MGB susceptibility map considered geology, geomorphology, distribution of sinkholes and other karst features, and proximity to lineaments in the identification of areas susceptible to subsidence. These, however, were assigned generally equal weights based on ground observations. Meanwhile, for the model presented, six (6) factors were identified to have influence significantly in the distribution of karst features based on the threshold for computed AUC values - that is above 60% (Table 3).

Factor Maps

Table 3. Calculated AUC values for the significant subsidence factors

Factor	AUC
Sink density	86.69%
Cave density	80.98%
Lineament density	74.52%
Geomorphology	71.13%
Landcover	63.26%
Geology	60.39%

Sink density, cave density, lineament density, land cover, geomorphology, and lithology are essential factors in the formation of sinkholes (Fig. 2). Sink density refers to the concentration of sinkholes within a specific region, providing insights into their spatial distribution and prevalence. Similarly, cave density denotes the abundance and clustering of underground cavities, which can contribute to sinkhole development. Lineament density examines the frequency and arrangement of linear features, such as faults and fractures, that may influence the occurrence of sinkholes. Land cover plays a crucial role by influencing hydrological processes and erosion, thereby impacting sinkhole formation. Geomorphology investigates the landforms and processes responsible for shaping the Earth's surface, including sinkhole genesis. Lastly, lithology examines the composition, structure, and physical properties of rocks, which can dictate the susceptibility of an area to sinkhole formation. Understanding the complex interplay between these factors is crucial for understanding the multifaceted nature of sinkhole development.

For the influence of each factor, sinkhole and cave density had the largest AUC values. Further, the clustering of sinkholes and caves,

in an area positively affected the computation. For lineaments, only the classes with lineament density greater than 0.89 sinks per square km had positive weights. In terms of geomorphology subsidence was more likely to occur along clastic hills, cockpit karst, and reef terrace. Tree cover and bare/sparsely vegetated areas were more like to experience subsidence. Then for geology, the limestone members of the Siargao Formation were identified to influence the susceptibility of an area.

The MGB Karst Subsidence Susceptibility Map (Fig. 3) delineated the whole municipality as highly susceptible to subsidence due to sinkhole collapse because of the presence of sinkholes (i.e., karst and pseudokarst), cave openings, as well as springs and wells, in all barangays. Delineation was also based on the underlying limestone and clastic formation, as well as the lineaments and observed localized faults, in the whole municipality. Anecdotal accounts and data on active seismicity and rainfall in the area were also considered.

The enhanced karst subsidence susceptibility map (Fig. 4) generated from the WoE method provided three (3) hazard susceptibility zonation within the municipality namely, moderate, high, and very high. These were identified based on the threshold values that corresponded to the percentage hazard pixels set for each classification (Table 4).

Multiple test runs were conducted using different training and testing subsets to obtain success and prediction rates based on the model, respectively. An initial test run using the available training data showed an initial success rate of 82.2% and another test revealed a success rate of 80.1%. Further tests produced success rates averaging to more than 80% and a prediction rate of 75.4% indicating a relatively good reliability based on available thematic and hazard datasets. The true positive (TPR) and false negative (FPR) rates were calculated following the equations below

Table 4. Sample values and the corresponding susceptibility zonation (Trial: SIAS-19).

Susceptibility	Values	0	1	True Positive Rate	False Positive Rate	Success Rate
Low	73	1006972	2081	0.921966674	0.319464533	80.13%
Moderate	80	567342	3904			
High	87	428216	27231			
Very High	100	310816	43482			

4. Conclusion

The MGB Geological Risk Reduction and Resiliency Program, along with the PhilKARST program, recognizes the importance of reliable and generally accurate hazard maps for government programs and plans, especially in land use and disaster risk management as well as sustainable tourism in karst areas. Thus, two (2) karst subsidence hazard susceptibility maps were generated in the process. The MGB-established methodology gave equal importance to the lithological distribution, subsurface and structural controls, as well as the climatological conditions in a more qualitative manner. On the other hand, the enhanced mapping methodology applied a more efficient statistics-based and data-driven process to consider the spatial distribution of karst features and karst-forming conditions to semi-automatically delineate and assign degrees of the susceptibility of areas that are vulnerable to subsidence through the inclusion of more factors. The latter produced success rates averaging to more than 80% and a prediction rate of 75.4% that entails relatively good method reliability. This approach also assures consistency and reproducibility. Hence, in contrast to that of previous methodology, the enhanced map generated through the WoE will be able to aid in the systematic identification and zoning of priority areas for development and recreation, settlement, protection, and hazard management.

Lastly, the results of the WoE method and the enhanced karst subsidence susceptibility map will be validated through follow-up fieldworks. This approach and its applicability to the mapping of the remaining targets under the NGAMP shall be explored. Expanding the size of the hazard inventory, as well as improving the resolution of the thematic factor maps, shall also be delved into.

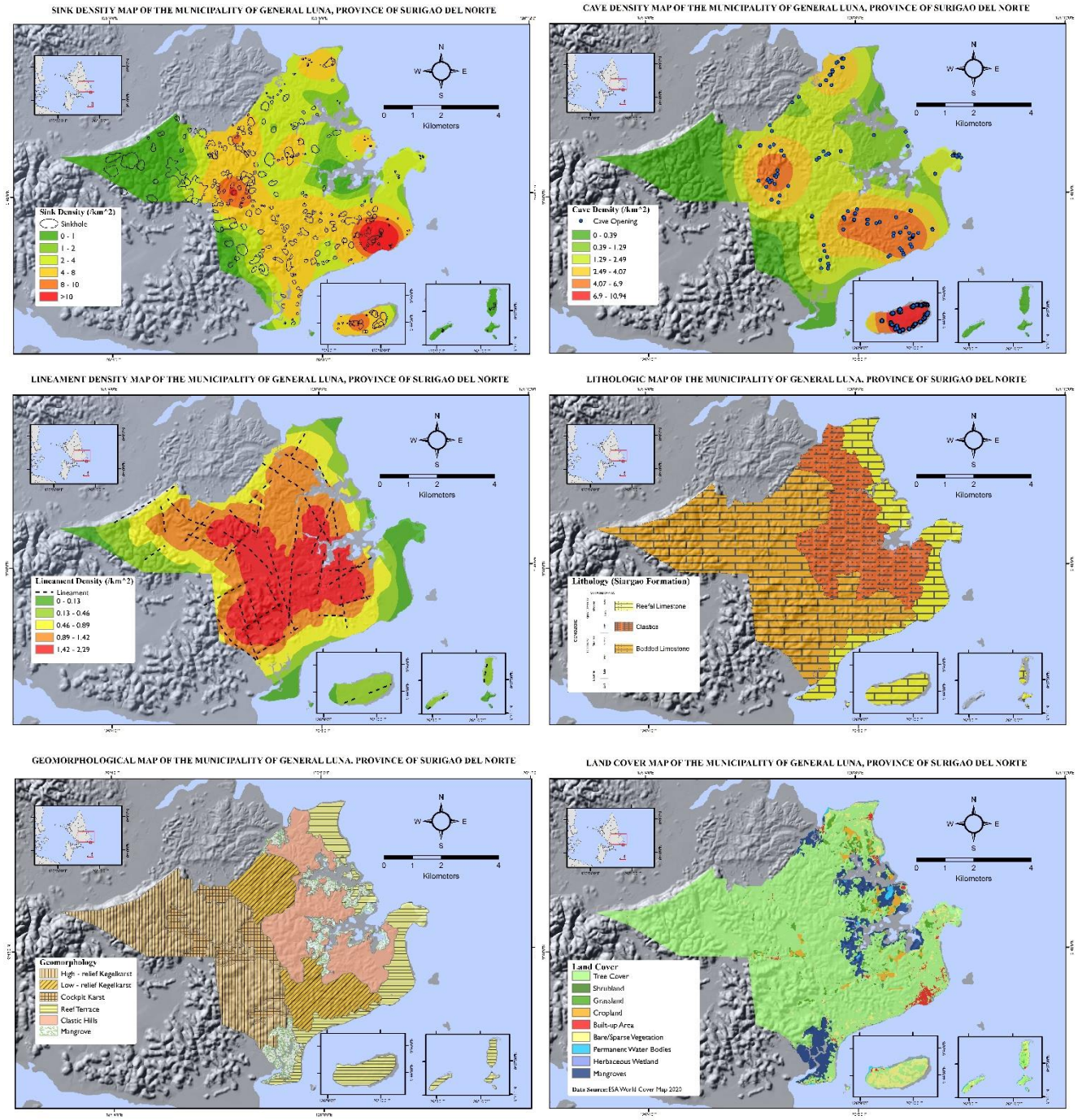

Fig. 2: Thematic maps of the factors used in the model. (Top left) Sink Density; (top right) cave density; (middle right) lineament density; (middle left) lithologic map; (bottom left) geomorphologic map; (bottom right) land cover

Karst Subsidence Susceptibility Maps

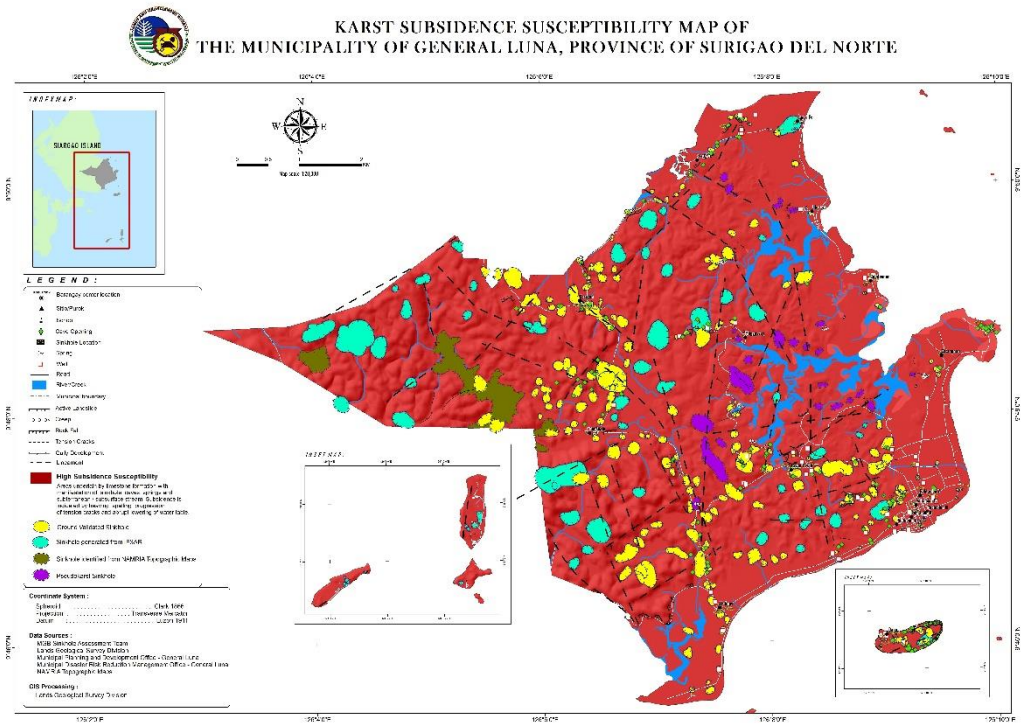

Fig. 3: Karst Subsidence Susceptibility Map of General Luna, Province of Surigao del Norte based on the MGB Karst Subsidence Hazards Assessment and Mapping Methodology. (Left) Enlarged Legend section.

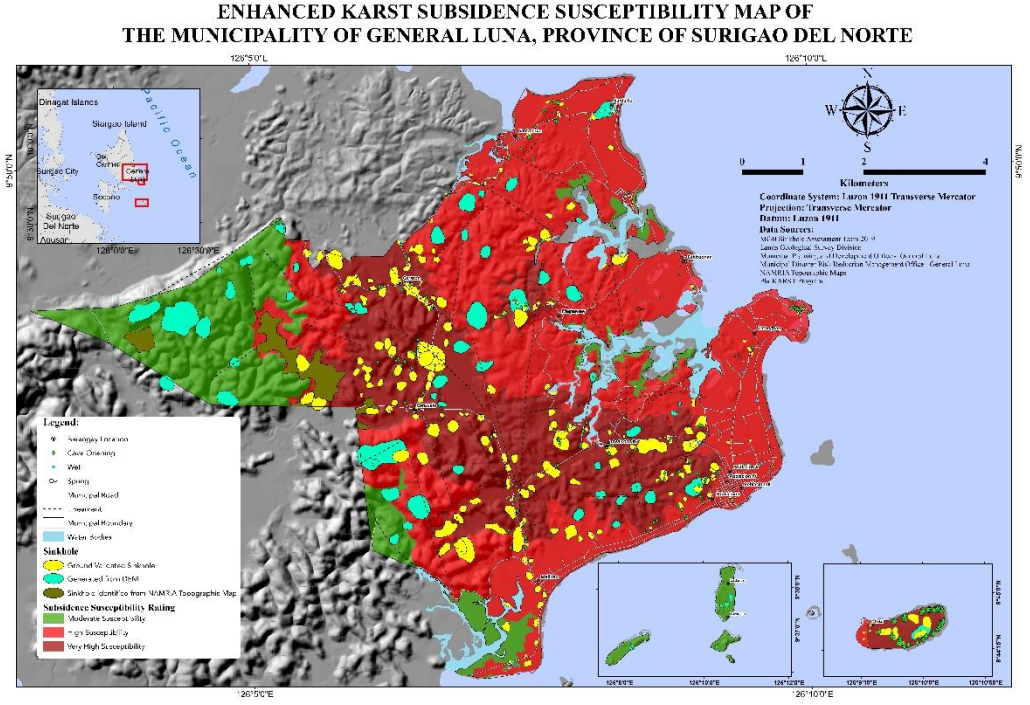

Fig. 4: Enhanced Karst Subsidence Susceptibility Map of General Luna, Province of Surigao del Norte based on the Weights of Evidence Analysis

Acknowledgment

The authors would like to thank the Department of Science and Technology - Philippine Council for Industry, Energy, and Emerging Technology Research and Development (DOST-PCIEERD) for providing the funding for this study. Lastly, the assistance of the local government unit of General Luna, whom the authors are grateful for their time and effort during the field assessment.

References

Fernandez, H. R. (1966). The Geology of Siargao Island, Surigao del Norte. (Unpublished report). Retrieved from: Bureau of Mines and Geosciences.

Garas, K. L., Madrigal, M., Agot, R. D. D., & Manzano, L. S. J. (2020). Karst depression detection using IFSAR-DEM:A tool for subsidence hazard assessment in Panglao, Bohol. ResearchGate.

Mines and Geosciences Bureau. (2010). Geology of the Philippines (2nd ed.). Manila, Philippines: Mines and Geosciences Bureau, Department of Environment and Natural Resources.

Mines and Geosciences Bureau. (2019). Technical Report on the Karst Subsidence Hazard Assessment and Ground Penetrating Radar (GPR) Survey in the Municipality of General Luna, Siargao Island, Surigao Del Norte. Unpublished report.

Mines and Geosciences Bureau. (2015). Karst Subsidence Hazard Susceptibility Assessment: A Guidebook. Unpublished manuscript.

Metal Mining Agency of Japan-Japan International Cooperation Agency (MMAJ-JICA). (1990). Consolidated Report on Samar, Leyte, Dinagat, Siargao Area: The Mineral Exploration – Mineral Deposits and Tectonics of Two Geologic Environments in the Republic of the Philippines. Available from https://openjicareport.jica.go.-jp/pdf/10804870_05.pdf

Perrin, J., Cartannaz, C., Noury, G., & Vanoudheusden, E. (2015). A multicriteria approach to karst subsidence hazard mapping supported by weights-of-evidence analysis. Engineering Geology, 197, 296–305.

Piccini, L., & Rossi, G. (1994). Italian caving exploration in the Island of Palawan, Philippines. (A. De Vivo, Trans.) Speleologia, 31, 5-61. Available from: https://www.research-gate.net/publication/274889717_Le_esplorazioni_speleologiche_italiane_nell'Isola_di_Palawan_Filippine__Italian_caving_exploration_in_the_island_of_Palawan_Philippines

Sadisun, I. A., Telaumbanua, J. A., Kartiko, R. D., Dinata, I. S., & Pamela. (2021). Weight of Evidence Method for landslide susceptibility mapping in Sigi Biromaru, Central Sulawesi. IOP Conference Series, 830(1), 012029.

Sumaryono, Muslim, D., Sulaksana, N., & DasaTriana, Y. (2015). Weights of Evidence Method for Landslide Susceptibility Mapping in Tandikek and Damar Bancah, West Sumatra, Indonesia. International Journal of Science and Research, 4, 1283-1290.